J Mol Model (2001) 7:288–305
DOI 10.1007/s008940100016

ORIGINAL PAPER

Wolfgang Förner · Hassan M. Badawi

Theoretical vibrational spectra of cyclohexanecarboxaldehyde

Received: 16 May 2000 / Accepted: 2 March 2001 / Published online: 23 August 2001

Abstract Vibrational spectra of cyclohexanecarboxaldehyde are calculated with density functional theory using the B3LYP functional together with a 6-311++G** basis set and presented. The results in the case of the infrared spectrum of the mixture of conformers at 300 K are compared with the experimental spectrum and, apart from the intensities of the CH and CO stretches, reasonable agreement is found. These deficiencies can be traced back to the well-known nonlinearities in case of CH stretches and the CO stretch. Potential energy distributions among symmetry coordinates in each normal mode are presented and used to assign specific atomic movements to each of the modes. Potential energy scans for the CHO rotor in both the *axial* and *equatorial* conformers are presented and barrier heights are compared with previous Hartree–Fock calculations and experimental data. It is reported that there could be three stable conformers, namely *equatorial-gauche* (*eg*), which is the most stable, *equatorial-trans* (*et*) and *axial-gauche* (*ag*). The optimized energies of all the minima and of the transition states are presented. However, comparison of the calculated spectrum with the experimental one indicates that total energies are slightly in error and that in the mixture of conformers no *ag* is present and thus the *et* to *eg* ratio is also different. Using experimental values for relative energies of conformers, we could obtain spectra in fair agreement with experiment. This indicates that when only total energy differences are calculated, slight errors in them play a role because of the very small relative energies in this case, while properties like geometries and spectra, which depend not on energy differences but on analytically calculated energy derivatives, are not affected.

Electronic supplementary material to this paper can be obtained by using the Springer link server located at http://dx.doi.org/10.1007/s008940100016.

W. Förner (✉) · H.M. Badawi
Department of Chemistry,
King Fahd University of Petroleum and Minerals,
Dhahran 31261, Saudi Arabia
e-mail: forner@kfupm.edu.sa

Keywords Cyclohexanecarboxaldehyde · Vibrational spectra · Potential energy distributions · Potential scans · Conformational stability

Introduction

The conformational stability of a series of saturated and unsaturated ring compounds of the general formula R–CXO has been investigated by ab initio calculations as well as by experimental techniques such as rotational and vibrational spectroscopy. [1, 2, 3, 4, 5, 6, 7, 8] Here R represents cyclopropane, cyclobutane, cyclopentene, cyclopentane, or cyclohexane rings, while X denotes hydrogen, fluorine, or chlorine. In the case of cyclopropane as R, the carbonyl oxygen was found to eclipse the three-membered ring in the gas phase as a result of a resonance stabilization, while it eclipses the ring hydrogen in the condensed phase because of the influence of intermolecular forces. [6] In contrast, in the unsaturated 3-cyclopropenecarboxaldehyde and its fluorine derivative, it was found that the lowest energy conformer is the one where the carbonyl oxygen eclipses the α-hydrogen (*trans* conformer) and not the ring. [8] This is due to the fact that in the latter case the frontier orbital interactions in the molecule have a destabilizing effect.

Higher order cyclic molecules with *N* atoms in the ring exhibit *N*–3 out-of-plane ring vibrations that determine the conformation of the ring. In the case of cyclobutanes the puckered ring with an equatorial substituent in the *gauche* conformation was found to be the most stable one. [1, 2, 3] The conformational behavior of 4-cyclopentenecarboxaldehyde is similar to that of cyclobutanecarboxaldehyde, both having the ring-puckering vibration as the only ring motion that gives rise to *axial* and *equatorial* conformations of the ring. In recent ab initio calculations, it was found that the molecule should exist as a complex mixture of *equatorial* and *axial* forms at ambient temperature. [9] From an ab initio calculation of the structures of cyclopentanecarboxaldehyde and cyclopentanecarbocylic acid fluoride, a twisted

ring with the substituent in the *gauche* conformation was predicted to be the lowest energy form of the compounds. [4, 5]

The conformational isomerism of cyclohexanecarboxaldehyde has been investigated by rotational spectroscopy. [10] Two stable isomers were found, both having the ring in a chair structure and *trans* and *gauche* conformations of the aldehyde substituent. No band series corresponding to an *axial* conformation could be identified. The data were in good agreement with recent ab initio calculations (Hartree–Fock, HF, and correlation calculations, such as MP2 and MP3). In these calculations the *gauche* conformer was found to be lower in energy than the *trans* one, [7] consistent with experimental data. [10]

In the present work we report calculated potential curves for the torsion of the aldehyde group as well as equilibrium geometries of the stable conformers and vibrational wavenumbers together with infrared and Raman intensities. Further, we have determined the distribution of the potential energy in the different normal modes among a set of motions defined by symmetry coordinates and report this potential energy distribution (PED). The infrared spectrum calculated at 300 K is compared to the experimental one. Fair agreement is found when the experimental relative energies of the conformers are used to determine their abundance in the mixture at 300 K.

Potential energy curves and equilibrium structures

The Gaussian98 program [11] running on an IBM RS/6000 P43 model 260-H70 workstation was used to carry out the necessary ab initio calculations. We used the 6-311++G** basis set, which is a valence triple zeta basis augmented with polarization and diffuse functions on hydrogen, carbon, and oxygen. As we will discuss below, this rather extended basis set gives some problems as far as total energy differences are concerned, but yields equilibrium geometries and spectra in fair agreement with experiment. The basis set was used generally for our calculations using density functional theory (DFT) together with the Becke 3 (B3) exchange and the Lee–Yang–Parr (LYP) correlation functional, as implemented in the program. [11] One has to note that in order to correct some shortcomings in the LYP functional, the program uses a combination of the LYP together with the Vosco–Nuzair–Wilks (VNW) correlation functional under the keyword B3LYP. [11]

In Fig. 1 we show a sketch of the *equatorial-trans* (*et*) conformation to define the atom numbering used throughout this text. A scan of the potential energy as function of the torsional angle φ suggested the presence of four energy minima, namely *equatorial-gauche* (*eg*), φ=64.3°, *equatorial-trans* (*et*), φ=180°, *axial-gauche* (*ag*), φ=72.6°, and *axial-trans* (*at*), together with four maxima, namely *equatorial-cis* (*ec*), the *eg*→*et* transition state (ets), the corresponding ats transition state and *axial-cis* (*ac*). The scans are plotted in Fig. 2a and b. We started out from the appropriate optimized *cis* form (*ec* and *ac*, respectively) and varied the aldehydic torsional angle φ, performing single point calculations at each value. The results are plotted in the two figures as solid lines. Then at the suggested extremal points we performed full geometry optimization and added the zero-point energies. These results are plotted as shaded circles. The optimizations had two immediate consequences. First of all *eg* becomes lower in energy than *et*, in agreement with experiment, and further the shallow *at* minimum changes to a maximum, leaving the *axial* curve with one minimum (*ag*) and two maxima (*ac*, *at*).

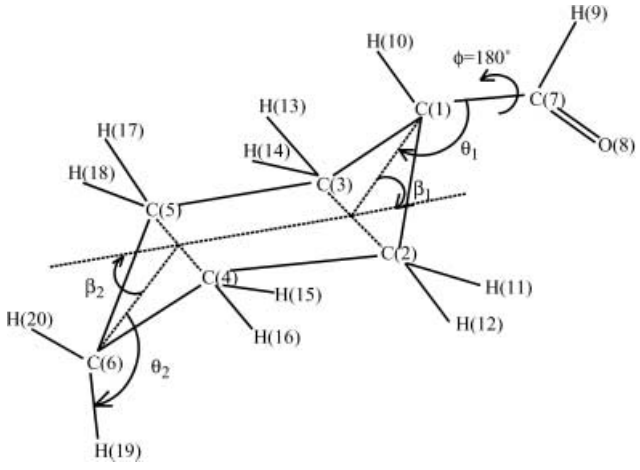

Fig. 1 Sketch of the molecular structure of the *equatorial-trans* conformer of cyclohexanecarboxaldehyde, defining the numbering of the atoms used later on

In Table 1 we show the optimized structural parameters for the three minima of the potential together with their experimental values. [10] For the sake of comparison we also show values of these parameters for the *et* conformer, obtained with the restricted Hartree–Fock (RHF) and the second order Møller–Plesset (MP2) method for the introduction of correlation corrections, using the same basis set. The mean square deviation between DFT results and experimental values is 0.009 Å for bond lengths and 2.5° for bond angles. Average mean square deviations for 32 molecules between DFT-BLYP results and experimental ones have been published [12] and are 0.020 Å for bond lengths and 2.33° for bond angles. Thus the deviations we obtain are roughly of the same order as experience would suggest. We conclude from this that the geometrical data we have obtained agree rather well with experiment. For the sake of comparison, in the *et* case the mean square deviations between MP2 and DFT are 0.005 Å and 0.89°, respectively. This is again evidence that DFT results are roughly as reliable as MP2 ones. Between RHF and DFT deviations are 0.011 Å and 0.25°.

Table 2 shows the resulting energies and relative energies, together with dipole moments and rotational constants for the extremal points we have located on the potential surface. While rotational constants are in reasonable agreement with their experimental values, [10] two major discrepancies immediately catch the eye when

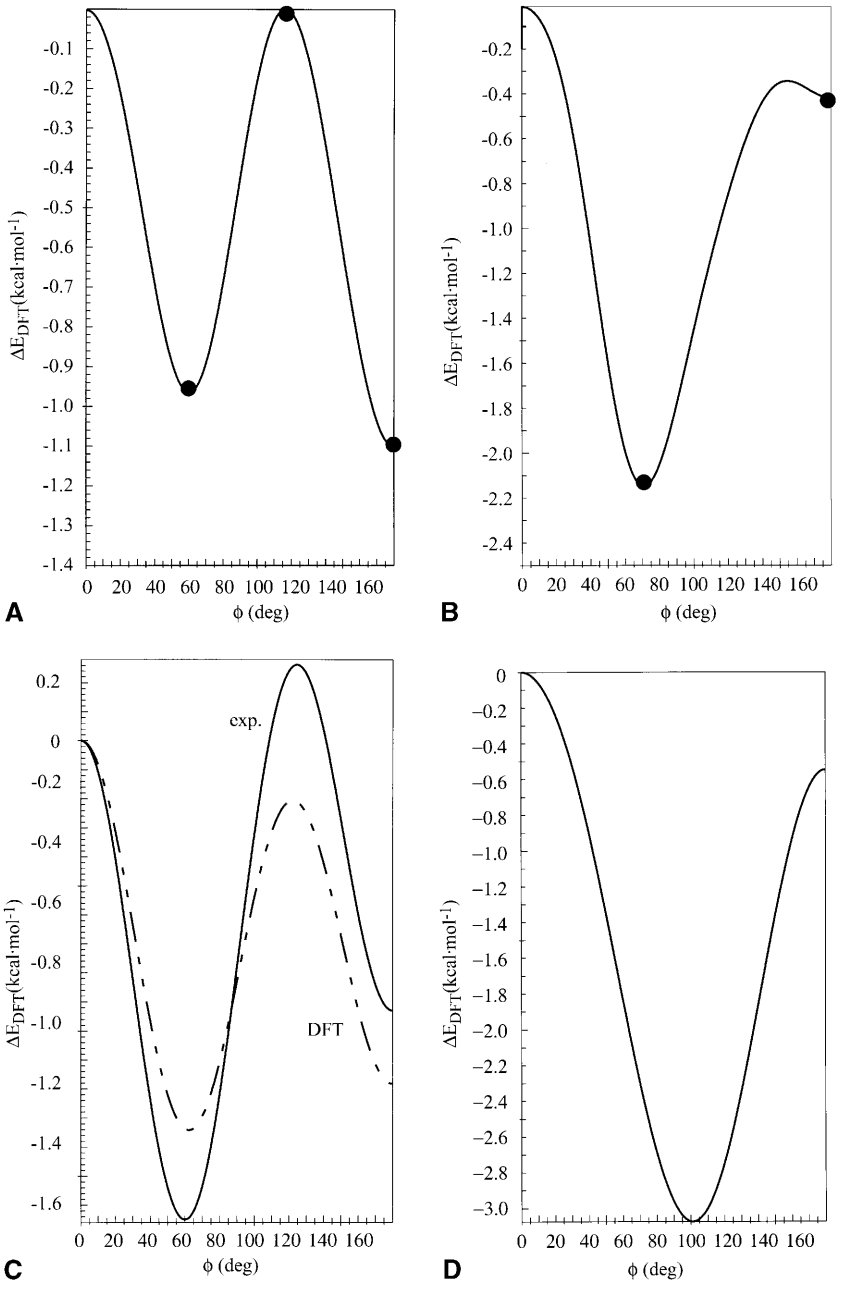

Fig. 2a–d Plots of the relative (to the respective *cis* maxima) potential energy (in kcal mol^{-1}) of cyclohexanecarboxaldehyde calculated with the help of the DFT method with the B3LYP functional. **a** Starting from the optimized *ec* geometry the torsional angle φ was varied and single point calculations performed for each of its values (solid line). Then for the suggested extrema full geometry optimizations were performed (shaded circles, zero-point energies included).**b** Starting from the optimized *ac* geometry the torsional angle φ was varied and single point calculations performed for each of its values (solid line). Then for the suggested extrema full geometry optimizations were performed (shaded circles, zero-point energies included).**c** Plots of a fit of a Fourier series to the optimized energy values (zero-point energies included) at the extrema obtained by DFT calculations (dashed line) and those obtained by rotational spectroscopy [10] (solid line). **d** Similar fit to the DFT data (optimized structures) for the *axial* form

looking at Table 2. First of all, there is no *ag* conformer found experimentally, suggesting that its energy should be much higher than our calculations predict. Further the energy difference of 0.16 kcal mol^{-1} for the *eg* and *et* conformers is much smaller than the experimental value of 0.72 kcal mol^{-1}. Also the *ec* maximum is in our calculations lower at 1.34 kcal mol^{-1} than found experimentally (1.65 kcal mol^{-1}). The same effect is seen in Fig. 2c, where Fourier fits of the extremal points are plotted for both the DFT (dashed line) and experimental values [10] (solid line). It is clear from the comparison that here we have the same problem. Figure 2d shows the corresponding *axial* case. In Table 3 the coefficients obtained in such fits are shown. It is obvious that the first order coefficient in eq_2 differs drastically from the corresponding one in the experimental fit, while the other two are in moderate agreement.

We now discuss why such a disagreement with experiment could appear, considering on the other hand the good agreement between geometrical data and experiment. Inspection of RHF outputs of all the conformers shows clearly where the reason lies. In all RHF outputs the Gaussian98 program issues a warning that large MO (molecular orbital) coefficients appear (104.6 in *eg* and 109.1 in *et*). Looking at the energy differences including zero-point energies between *eg* and *et* for RHF calculations in different basis sets we have the sequence 1.50, 0.57, 0.50, and 0.14 kcal mol^{-1} for the basis sets 3-21G (96 basisfunctions), 6-31G* (136 basisfunctions), [7] 6-311G* (180 basisfunctions), [13] and 6-311++G**

Table 1 Optimized structural parameters (see Fig. 1 for atom numbering and denotation of the symbols used for some of the parameters) of cyclohexanecarboxaldehyde for the three stable conformers, i.e. *equatorial-trans* (*et*), *equatorial-gauche* (*eg*) and *axial-gauche* (*ag*), calculated with different methods (RHF, MP2 and DFT), but all using the same basis set (6-311++G**). The experimental values (column headed "exp.") are taken from [10]

Parameter	et RHF	et MP2	et DFT	eg DFT	ag DFT	exp
Bond lengths (Å)						
C(1) C(2)	1.538	1.538	1.546	1.544	1.544	1.526
C(2) C(4)	1.531	1.532	1.535	1.536	1.536	1.526
C(4) C(6)	1.530	1.531	1.534	1.536	1.535	1.526
C(7) C(1)	1.508	1.506	1.510	1.513	1.519	1.501
C(7) O(8)	1.184	1.217	1.207	1.207	1.206	1.216
C(7) H(9)	1.100	1.114	1.115	1.114	1.115	1.114
C(1) H(10)	1.086	1.098	1.095	1.104	1.102	1.096
C(2) H(11)	1.090	1.100	1.098	1.097	1.096	1.096
C(4) H(15)	1.087	1.096	1.095	1.095	1.098	1.096
C(6) H(19)	1.090	1.099	1.098	1.098	1.095	1.096
Bond angles (deg)						
C(2) C(1) C(3)	110.8	110.4	110.8	111.7	112.2	112.3
C(4) C(6) C(5)	111.3	110.9	111.3	111.5	111.2	112.3
C(1) C(7) O(8)	125.1	125.2	125.4	125.5	125.9	123.9
C(1) C(7) H(9)	115.1	114.5	114.6	114.5	114.2	117.5
C(1) C(2) H(11)	109.3	109.0	109.2	108.8	110.1	
C(6) C(4) H(15)	110.3	110.5	110.4	110.3	109.1	
H(11) C(2) H(12)	106.8	107.2	106.7	106.8	106.4	
H(15) C(4) H(16)	106.6	107.0	106.5	106.5	106.3	
H(19) C(6) H(20)	106.6	107.0	106.5	106.5	106.5	106.7
C(7) C(1) H(10)	107.0	107.5	107.2	104.7	103.3	
θ_1	127.2	126.1	126.9	131.9	132.7	
θ_2	125.9	125.3	125.8	125.7	127.6	
β_1	49.6	50.6	49.2	49.6	46.1	52.4
β_2	49.4	50.8	49.3	49.3	50.1	52.4
Dihedral angles (deg)						
H(10) C(1) C(2) C(4)	114.3	114.8	113.7	115.9	9.6	
H(11) C(2) C(4) C(6)	114.2	116.1	114.1	114.4	3.3	
O(8) C(7) C(1) H(10)	180.0	180.0	180.0	64.3	72.6	60.0

Table 2 Total energies, E_{DFT}, and zero-point energies, E_0, (in H), relative energies, ΔE (relative to *equatorial-gauche*, *eg*), in kcal mol^{-1}, total dipole moments μ in Debye, rotational constants (*A*, *B*, and *C*) in GHz and barriers to internal rotation, ΔE (*et*→*eg*) and ΔE (*eg*→*et*) through ets, in kcal mol^{-1}. Experimental data are taken from [10]. In the denotations of the conformers *e* denotes *equatorial*, *a axial*, *c cis*, *t trans*, *g gauche*, and ts transition state. *eg*, *et* and *ag* represent minima, all others are maxima

Conformer	E_{DFT}	E_0	ΔE		μ	A		B		C		ΔE	
			DFT	exp		DFT	exp	DFT	exp	DFT	exp	DFT	exp
eg	–349.295864	0.178262	0.00	0.00	3.02	3.948	3.952	1.410	1.424	1.123	1.137	*eg*→*et* 1.13 *et*→*eg*	1.89
et	–349.295787	0.178435	0.16 (HF: 0.14)	0.72	3.37	4.111	4.132	1.317	1.328	1.081	1.090	0.97	1.17
ec	–349.293719	0.178251	1.34	1.65	2.83	3.797		1.439		1.190			
ets	–349.294048	0.178251	1.13		3.16	4.076		1.343		1.084			
ag	–349.294532	0.178482	0.97 (HF: 1.15)		2.79	3.014		1.741		1.456			
ac	–349.290611	0.178388	3.38		2.50	2.822		1.820		1.651			
at	–349.291492	0.178401	2.83		3.36	3.440		1.493		1.267			

(260 basisfunctions, this work), respectively. Only in the last of these basis sets do warnings about large MO coefficients appear, and we observe a drastic fall of the relative energy after a series of three values, converging smoothly with increasing size of the basis set. Such large MO coefficients usually suggest that there are linear dependencies in our basis set. Such warnings do not appear in the DFT calculations. However, here we also expect small errors in total energy due to basis set problems.

Such errors will have a dramatic effect on the relative energies of different conformers, especially in our case, with the experimental barrier being as low as 0.72 kcal mol^{-1}. Keeping in mind that in order to obtain such relative energies, one has to subtract two total ener-

Table 3 Coefficients V_k (in kcal mol^{-1}) for fits of potential energies as functions of the torsional angle φ of the CHO group to the Fourier series $\Delta E(\phi) = V_0 + \sum_k \frac{1}{2} V_k [1 - cos(k\phi)]$ where the fitted potential energies are relative to their value at φ = 0. The first two columns (equatorial$_1$ and axial$_1$) are the fits of the DFT energies as shown in Fig. 2a and b, the second and third columns (eq$_2$ and ax$_2$) are fits to four points each, which are obtained by full geometry optimizations at the extremal points, including the zero point vibrational energies. The fifth column (exp) gives a corresponding fit of experimental results from [10] (accuracy roughly 0.2 kcal mol^{-1})

k	eq$_1$	ax$_1$	eq$_2$	ax$_3$	exp
0	–0.003	–0.126	0.000	0.000	0.000
1	–0.144	0.384	–0.036	–0.978	0.640
2	0.111	–1.677	–0.249	–2.687	–0.320
3	–1.002	–0.898	–1.146	0.434	–1.570
4	–0.247	0.070			
5	0.478	0.108			
6	0.175	0.110			
root mean square deviations:					
	0.004	0.007	0.000	0.000	0.000
total energies at *cis* positions:					
	–349.293719 H	–349.290611 H	–349.115468 H	–349.112210 H	

gies from each other, which are of the order of 0.2 Gcal mol^{-1} to yield just a value of the order of a kcal mol^{-1} or less. From this it is obvious that the slightest irregularities in the basis set could affect such relative energies drastically, which is what actually happens here.

On the other hand, properties like equilibrium geometries, vibrational wavenumbers, and spectral intensities are not calculated by forming differences of large numbers, but are obtained from analytically calculated derivatives of the total energy. Thus we expect that only relative energies are affected by the basis set problem, while other properties are not, as we have seen already in case of the equilibrium geometries.

Potential energy distributions

The molecule in the symmetric *trans* conformation has C_s symmetry. Thus, the 54 vibrational modes span the irreducible representations: 31 A' and 23 A". The A' modes should be polarized in the Raman spectrum of the liquid. The *gauche* conformer has C_1 symmetry and therefore all the vibrational modes belong to the A representation and should be polarized in the Raman spectrum of the liquid.

We carried out normal coordinate analyses for the *eg*, *et*, and *ag* conformers of the molecule to provide an assignment of the fundamental vibrational wavenumbers to the types of atomic motion occurring in the molecule. For this end we followed Wilson's textbook, [14] The Cartesian coordinates of the stable conformers were taken together with the normal modes (in Cartesian coordinates) and their corresponding wavenumbers from the output of the Gaussian98 program. An overcomplete set of internal coordinates (Table 4) was used to set up symmetry coordinates (Table 5) for the molecule. The set of internal coordinates is overcomplete, just to make it easier to build the required atomic motions for the symmetry coordinates. The redundant internal coordinates are detected and removed automatically by our program (see the Appendix for a short outline of the procedure), both from the set of internal and symmetry coordinates. Further, it is checked that the remaining independent internal coordinates form a complete set that can be used to construct all possible internal motions of the molecule. Note that in Table 4 the internal coordinate I(61) for the aldehydic torsion is not a primitive torsional coordinate, but a combined one, so that it describes the rotation of the CHO group as a whole.

The normal modes were transformed to mass-weighted Cartesian coordinates, which were then used to calculate the force constant matrix. Following this step, the force constant matrix in mass weighted Cartesian coordinates was transformed to the force constant matrix in internal coordinates, which was then finally transformed to symmetry coordinates. In the program all these transformation steps were automatically checked in both directions. In the next step the normal modes were also transformed from Cartesian to symmetry coordinates. Together with the vibrational wavenumbers, the force constant matrix and the normal coordinate coefficients, both in symmetry coordinate space, were used to calculate the distribution of potential energy in a normal mode among all the symmetry coordinates (PED). The results for the three stable conformers are given in Table 6. The table gives the wavenumber *k* of all the modes together with a numbering and the symmetry label. Infrared intensities and Raman activities, together with the depolarization factors and the assignment to the symmetry coordinates in % of the total potential energy due to the symmetry coordinates in each normal mode, are also given.

At this point we would like to discuss some of the assignments in more detail because the structure and conformational behaviors of substituted cyclohexanes have been of interest for many years. [15, 16, 17, 18, 19, 20, 21, 22] The conformational equilibrium of halocyclohex-

Table 4 Internal coordinate definitions (for atom denotation see Fig. 1) for cyclohexanecarboxaldehyde

Coordinate	Definition
C(1) C(3)	stretch I(1)
C(1) C(2)	stretch I(2)
C(2) C(4)	stretch I(3)
C(4) C(6)	stretch I(4)
C(5) C(6)	stretch I(5)
C(3) C(5)	stretch I(6)
C(1) C(7)	stretch I(7)
C(1) H(10)	stretch I(8)
C(2) H(11)	stretch I(9)
C(2) H(12)	stretch I(10)
C(4) H(15)	stretch I(11)
C(4) H(16)	stretch I(12)
C(6) H(19)	stretch I(13)
C(6) H(20)	stretch I(14)
C(5) H(17)	stretch I(15)
C(5) H(18)	stretch I(16)
C(3) H(13)	stretch I(17)
C(3) H(14)	stretch I(18)
C(7) O(8)	stretch I(19)
C(7) H(9)	stretch I(20)
C(2) C(1) C(3)	bend I(21)
C(4) C(2) C(1)	bend I(22)
C(6) C(4) C(2)	bend I(23)
C(5) C(6) C(4)	bend I(24)
C(3) C(5) C(6)	bend I(25)
C(1) C(3) C(5)	bend I(26)
H(11) C(2) H(12)	bend I(27)
H(15) C(4) H(16)	bend I(28)
C(7) C(1) H(10)	bend I(29)
H(19) C(6) H(20)	bend I(30)
H(19) C(6) H(20)	bend I(30)
H(17) C(5) H(18)	bend I(31)
H(13) C(3) H(14)	bend I(32)
C(7) C(1) C(2)	bend I(33)
C(7) C(1) C(3)	bend I(34)
C(2) C(1) H(10)	bend I(35)
C(3) C(1) H(10)	bend I(36)
C(1) C(2) H(11)	bend I(37)
C(4) C(2) H(11)	bend I(38)
C(1) C(2) H(12)	bend I(39)
C(4) C(2) H(12)	bend I(40)
C(2) C(4) H(15)	bend I(41)
C(6) C(4) H(15)	bend I(42)
C(2) C(4) H(16)	bend I(43)
C(6) C(4) H(16)	bend I(44)
C(4) C(6) H(19)	bend I(45)
C(5) C(6) H(19)	bend I(46)
C(4) C(6) H(20)	bend I(47)
C(5) C(6) H(20)	bend I(48)
C(6) C(5) H(17)	bend I(49)
C(3) C(5) H(17)	bend I(50)
C(6) C(5) H(18)	bend I(51)
C(3) C(5) H(18)	bend I(52)
C(1) C(3) H(13)	bend I(53)
C(5) C(3) H(13)	bend I(54)
C(1) C(3) H(14)	bend I(55)
C(5) C(3) H(14)	bend I(56)
C(1) C(7) O(8)	bend I(57)
C(1) C(7) H(9)	bend I(58)
H(9) C(7) O(8)	bend I(59)
H(9) C(7) C(1) O(8)	wag I(60)
[H(9) C(7) C(1) H(10)+O(8) C(7) C(1) H(10)+H(9) C(7) C(1) C(2)+O(8) C(7) C(1) C(2)+H(9) C(7) C(1) C(3)+O(8) C(7) C(1) C(3)]	torsion I(61)

anes, for example, has been investigated by a variety of theoretical and experimental methods. [19, 20, 22] Fluoro-, chloro-, bromo-, and iodocyclohexanes have been studied and the *equatorial* conformation of all these molecules was determined to be the lowest energy form in the condensed phase. The corresponding aldehyde compound ($C_7H_{12}O$) has been studied by microwave spectroscopy and both identified conformers (*trans* and *gauche*) could be shown to have the aldehydic substituent in the *equatorial* position, just as in the halocyclohexanes. From relative intensity measurements, the *gauche* form was determined to be by 0.72 kcal mol^{-1} more stable than the *trans* conformer, and the rotational barrier height, corresponding to the *cis* position of the CHO group, was found to be above 1.70 kcal mol^{-1}. [10] This is consistent with earlier ab initio calculations. [7] Our DFT results do not agree with experiment, as far as relative energies are concerned, as discussed above. However, spectral properties should still be described well.

Theoretically, 12 of the 54 fundamentals are CH stretches, one of which is from the aldehydic group. All these stretches were calculated to have the highest Raman activities for all the conformers. In the following, *gauche* and *trans* refer to the *eq* and *et* conformations, respectively. The lowest calculated wavenumber of the CH stretches is the aldehydic CH stretch at 2849 cm^{-1} (*eg*) in moderate agreement with the corresponding one observed at 2731 cm^{-1} in the Raman spectrum of cyclobutanecarboxaldehyde. [3] Note that, as discussed below, wavenumbers of CH stretches are more in error than those of other vibrations due to anharmonicities in their potentials. In the ring CH stretching and bending modes we see that their potential energy is distributed over quite a few symmetry coordinates. Thus, there is a tremendous mixing of motions in each mode, with one exception, the α-CH stretch, which appears almost pure at 2951 cm^{-1} in the *gauche* conformer. This is not the case in the other conformers, where α-CH stretch appears mixed with other motions throughout. However, the α-CH stretch is the dominant contribution to mode number 49 in the *trans* conformer (73%) at 3038 cm^{-1}. As one sees in Table 6, but also in the spectra discussed below, the most intense Raman lines in the spectra of all the conformers are the ring breathing modes. These appear at 760 cm^{-1} [47% S(25)] in the *gauche* conformer and at 801 cm^{-1} (49%) in *trans*. This result agrees fairly well with the line observed at 797 cm^{-1} in liquid fluorocyclohexane. [20]

The assignments of the vibrational modes associated with the aldehydic group can be based on their PED values and on comparison with the corresponding ones in cyclobutanecarboxaldehyde. [3] The CO stretching mode appears nearly pure (91%) in the *gauche* conformer at 1795 cm^{-1} and at 1794 cm^{-1} (91%) in *trans*. This is consistent with the line observed at 1739 cm^{-1} in cyclobutanecarboxaldehyde. [3] As also found there, this line is the strongest feature in the infrared spectrum. The CC stretch in cyclobutanecarboxaldehyde was assigned to

Table 5 Symmetry coordinates (S, not normalized) for cyclohexanecarboxaldehyde

Species A' in *trans* or A in *gauche* conformers	
S(1)=I(7)	C–C stretch
S(2)=I(8)	α-CH symmetric stretch
S(3)=I(9)–I(10)+I(17)–I(18)	β-CH_2 antisymmetric stretch
S(4)=I(9)+I(10)+I(17)+I(18)	γ-CH_2 symmetric stretch
S(5)=I(11)–I(12)+I(15)–I(16)	γ-CH_2 antisymmetric stretch
S(6)=I(11)+I(12)+I(15)+I(16)	γ-CH_2 symmetric stretch
S(7)=I(13)–I(14)	δ-CH_2 antisymmetric stretch
S(8)=I(13)+I(14)	δ-CH_2 symmetric stretch
S(9)=I(20)	C–H_{ald} stretch
S(10)=I(19)	C=O stretch
S(11)=2×I(29)–I(35)–I(36)	α-CH in-plane bend
S(12)=4×I(27)–I(37)–I(38)–I(39)–I(40) +4×I(32)–I(53)–I(54)–I(55)–I(56)	β-CH_2 deformation
S(13)=I(37)–I(38)+I(39)–I(40)+I(53)–I(54)+I(55)–I(56)	β-CH_2 wag
S(14)=I(37)–I(38)–I(39)+I(40)+I(53)–I(54)–I(55)+I(56)	β-CH_2 twist
S(15)=I(37)+I(38)–I(39)–I(40)+I(53)+I(54)–I(55)–I(56)	β-CH_2 rock
S(16)=4×I(28)–I(41)–I(42)–I(43)–I(44) +4×I(31)–I(49)–I(50)–I(51)–I(52)	γ-CH_2 deformation
S(17)=I(41)–I(42)+I(43)–I(44)–I(49)+I(50)–I(51)+I(52)	γ-CH_2 wag
S(18)=I(41)–I(42)–I(43)+I(44)–I(49)+I(50)+I(51)–I(52)	γ-CH_2 twist
S(19)=I(41)+I(42)–I(43)–I(44)+I(49)+I(50)–I(51)–I(52)	γ-CH_2 rock
S(20)=4×I(30)–I(45)–I(46)–I(47)–I(48)	δ-CH_2 deformation
S(21)=I(45)+I(46)–I(47)–I(48)	δ-CH_2 rock
S(22)=I(58)–I(59)	C–H_{ald} in-plane bend
S(23)=I(58)+I(59)–2×I(57)	CCO in-plane bend
S(24)=3×I(33)+3×I(34)–2×I(29)–2×I(35)–2×I(36)	ring-CHO bend
S(25)=I(1)+I(2)+I(3)+I(4)+I(5)+I(6)	ring breathing
S(26)=I(1)+I(2)–2×I(3)+I(4)+I(5)–2×I(6)	ring deformation
S(27)=I(1)+I(2)–I(4)–I(5)	ring deformation
S(28)=I(21)+I(22)+I(23)+I(24)+I(25)+I(26)	ring symmetric puckering
S(29)=I(21)–I(22)+I(23)–I(24)+I(25)–I(26)	ring antisymmetric deformation
S(30)=2×I(21)–I(22)–I(23)+2×I(24)–I(25)–I(26)	ring symmetric deformation
S(31)=2×I(21)+I(22)–I(23)–2×I(24)–I(25)+I(26)	ring antisymmetric puckering
Species A" in *trans* or A in *gauche* conformers	
S(32)=I(35)–I(36)	α-CH out-of-plane bend
S(33)=I(9)–I(10)–I(17)+I(18)	β-CH_2 antisymmetric stretch
S(34)=I(9)+I(10)–I(17)–I(18)	β-CH_2 symmetric stretch
S(35)=I(11)–I(12)–I(15)+I(16)	γ-CH_2 antisymmetric stretch
S(36)=I(11)+I(12)–I(15)–I(16)	γ-CH_2 symmetric stretch
S(37)=4×I(27)–I(37)–I(38)–I(39)–I(40)–4×I(32) +I(53)+I(54)+I(55)+I(56)	β-CH_2 deformation
S(38)=I(37)–I(38)+I(39)–I(40)–I(53)+I(54)–I(55)+I(56)	β-CH_2 wag
S(39)=I(37)–I(38)–I(39)+I(40)–I(53)+I(54)+I(55)–I(56)	β-CH_2 twist
S(40)=I(37)+I(38)–I(39)–I(40)–I(53)–I(54)+I(55)+I(56)	β-CH_2 rock
S(41)=4×I(28)–I(41)–I(42)–I(43)–I(44)–4×I(31)+I(49) +I(50)+I(51)+I(52)	γ-CH_2 deformation
S(42)=I(41)–I(42)+I(43)–I(44)+I(49)–I(50)+I(51)–I(52)	γ-CH_2 wag
S(43)=I(41)–I(42)–I(43)+I(44)+I(49)–I(50)–I(51)+I(52)	γ-CH_2 twist
S(44)=I(41)+I(42)–I(43)–I(44)–I(49)–I(50)+I(51)+I(52)	γ-CH_2 rock
S(45)=I(45)–I(46)+I(47)–I(48)	δ-CH_2 deformation
S(46)=I(45)–I(46)–I(47)+I(48)	δ-CH_2 twist
S(47)=I(1)–I(2)+I(3)–I(4)+I(5)–I(6)	ring deformation
S(48)=I(1)–I(2)+I(4)–I(5)	ring deformation
S(49)=I(1)–I(2)–2×I(3)–I(4)+I(5)+2×I(6)	ring deformation
S(50)=I(22)–I(23)+I(25)–I(26)	ring antisymmetric deformation
S(51)=I(22)+I(23)–I(25)–I(26)	ring twisting
S(52)=I(60)	C–H_{ald} out-of-plane bend (wag)
S(53)=I(33)–I(34)	ring-CHO out-of-plane bend
S(54)=I(61)	CHO antisymmetric torsion (=φ)

the polarized and strong line at 1020 cm^{-1} in the Raman spectra of both the gas and the liquid. [3] This mode appears with a PED of 84% S(47) at 1090 cm^{-1} in the *trans* form and with a higher degree of mixing between symmetry coordinates with 58% S(47) at 1091 cm^{-1} in the *gauche* Raman spectrum. In case of the CHO bending, there are actually two modes of different symmetries in the *trans* conformer. The CH in-plane bend is of A' symmetry and appears with 80% S(22) at 1419 cm^{-1} in the *gauche* conformer and at 1413 cm^{-1} with 82% in the *trans* form of the molecule. In the infrared spectrum of cyclobutanecarboxaldehyde it was observed at

Table 6 Numbers *i* of vibrations in order of increasing wavenumbers, symmetry species S_p, wavenumbers *k* ($k=1/\lambda$, in cm^{-1}, DFT results), infrared intensities *I* (in K m mol^{-1}, equivalent to 6.161×10^{-22} W m^{-2} Hz^{-1}, where 1 mol corresponds to 22.41 dm^3 at Standard Temperature and Pressure, while 1 K corresponds to 1.381×10^{-23} J, DFT results), Raman activities *S* (in $Å^4$ amu^{-1}), depolarization ratios ρ (both *S* and ρ values are from DFT), and the contributions of the different symmetry coordinates S(*l*) to the Potential Energy Distribution (PED) for each normal mode (only contributions larger than or equal to 10% are listed, DFT results) for the three stable conformers of cyclohexane carboxaldehyde (6-311++G** basis set in all calculations, B3LYP functional in all DFT calculations). The total energies, E_{tot}, include the zero-point energies (in brackets the percentage in the mixture of conformers at 300 K is given)

i	S_p	*k*	I	S	ρ	PED
equatorial-gauche (63.3%) E_{tot} =–349.117602 H						
1	A	71	5.85	1.06	0.75	68% S(54) 16% S(24)
2	A	143	2.51	0.61	0.73	56% S(31) 14% S(54) 12% S(24)
3	A	215	3.56	0.46	0.67	35% S(51) 31% S(53) 11% S(49) 11% S(23)
4	A	232	3.29	0.24	0.58	51% S(51) 22% S(53)
5	A	316	0.32	0.57	0.73	39% S(28) 20% S(24) 20% S(31)
6	A	356	0.28	3.53	0.23	36% S(30) 14% S(1) 10% S(24) 10% S(28)
7	A	412	1.27	0.89	0.11	36% S(30) 29% S(28) 10% S(24)
8	A	438	0.23	0.91	0.75	80% S(50)
9	A	506	0.57	0.57	0.13	40% S(29) 14% S(19) 11% S(21) 10% S(15)
10	A	677	17.35	3.02	0.50	43% S(23) 10% S(24) 10% S(49)
11	A	760	3.73	18.89	0.09	47% S(25) 10% S(19)
12	A	795	0.17	0.81	0.75	41% S(40) 38% S(44) 12% S(48)
13	A	839	0.41	4.87	0.07	51% S(27) 24% S(25)
14	A	849	1.64	1.33	0.55	41% S(21) 25% S(15)
15	A	900	4.07	0.57	0.73	39% S(49) 15% S(44) 12% S(40)
16	A	924	5.48	0.10	0.33	26% S(44) 23% S(40) 14% S(49)
17	A	945	10.49	1.96	0.68	17% S(1) 15% S(27) 10% S(52)
18	A	970	7.85	2.99	0.68	25% S(52) 21% S(19)
19	A	1035	0.23	11.98	0.74	64% S(26) 12% S(17) 10% S(13)
20	A	1057	1.45	5.76	0.74	25% S(48) 19% S(29)
21	A	1074	2.97	1.13	0.65	19% S(43) 19% S(39) 13% S(32)
22	A	1091	0.07	0.79	0.55	58% S(47) 12% S(42)
23	A	1113	4.36	1.68	0.69	24% S(47) 19% S(39)
24	A	1164	2.69	3.73	0.15	29% S(15) 19% S(19) 15% S(21) 10% S(28)
25	A	1210	3.43	3.67	0.75	28% S(43) 17% S(38) 13% S(48)
26	A	1258	1.56	4.84	0.69	30% S(18) 24% S(11) 13% S(13)
27	A	1282	0.33	2.02	0.75	35% S(46) 19% S(32) 10% S(39)
28	A	1293	1.38	10.74	0.75	67% S(14)
29	A	1312	2.48	8.35	0.75	25% S(18) 18% S(39) 16% S(11) 15% S(32)
30	A	1327	4.95	1.79	0.54	18% S(18) 18% S(38) 15% S(11) 12% S(32)
31	A	1356	0.78	2.57	0.67	38% S(38) 11% S(32) 10% S(42)
32	A	1366	0.05	0.75	0.68	52% S(42) 16% S(46)
33	A	1377	0.23	0.44	0.68	56% S(45) 12% S(43)
34	A	1379	0.54	1.73	0.75	66% S(17) 12% S(14)
35	A	1389	5.49	3.43	0.28	54% S(13)
36	A	1419	3.23	3.52	0.65	80% S(22)
37	A	1484	0.54	15.91	0.75	70% S(37) 25% S(41)
38	A	1486	5.00	10.02	0.75	69% S(20) 22% S(12)
39	A	1488	5.31	0.31	0.72	71% S(41) 27% S(37)
40	A	1493	14.59	0.03	0.05	61% S(16) 34% S(12)
41	A	1505	1.09	0.67	0.70	40% S(12) 34% S(16) 24% S(20)
42	A	1795	211.66	16.42	0.50	91% S(10)
43	A	2849	136.02	108.74	0.41	99% S(9)
44	A	2951	18.18	82.25	0.17	97% S(2)
45	A	2997	18.57	85.29	0.22	27% S(6) 24% S(36) 15% S(8) 13% S(5)
46	A	3000	17.29	153.95	0.22	43% S(36) 12% S(8) 11% S(35)
47	A	3006	11.42	78.40	0.24	29% S(34) 25% S(4) 23% S(8)
48	A	3008	41.66	49.32	0.26	31% S(6) 31% S(8) 19% S(34) 10% S(4)
49	A	3025	16.51	66.36	0.24	48% S(4) 29% S(34)
50	A	3046	52.38	70.56	0.60	37% S(3) 37% S(33)
51	A	3051	56.59	107.08	0.32	39% S(35) 31% S(7)
52	A	3052	37.56	215.18	0.18	36% S(35) 19% S(7) 10% S(5) 10% S(6)
53	A	3057	78.77	107.85	0.22	58% S(5) 24% S(7)
54	A	3075	34.23	80.57	0.34	45% S(3) 38% S(33)
equatorial-trans (24.3%) E_{tot}=–349.117352 H						
1	A”	60	7.20	1.70	0.75	82% S(54) 11% S(53)
2	A’	111	2.54	0.12	0.75	58% S(31) 23% S(24) 10% S(28)
3	A”	220	0.01	0.00	0.75	91% S(51)

Table 6 (continued)

i	S_p	*k*	I	S	ρ	PED
4	A”	291	1.18	1.74	0.75	70% S(53) 14% S(54)
5	A’	293	2.58	0.86	0.45	35% S(31) 20% S(28) 13% S(24) 10% S(23)
6	A’	354	0.06	2.16	0.38	50% S(30) 12% S(1) 10% S(28)
7	A’	403	4.12	1.92	0.01	46% S(28) 22% S(24)
8	A”	444	0.18	1.11	0.75	79% S(50)
9	A’	513	0.43	3.04	0.07	24% S(29) 18% S(30) 10% S(19)
10	A’	566	14.35	1.25	0.28	40% S(23) 19% S(29)
11	A”	792	0.00	0.85	0.75	40% S(44) 39% S(40) 14% S(48)
12	A’	801	0.79	17.09	0.07	49% S(25) 16% S(15)
13	A’	844	0.66	2.61	0.11	36% S(27) 25% S(21) 18% S(25)
14	A”	870	0.90	0.52	0.75	68% S(49) 12% S(52)
15	A’	899	0.90	1.36	0.19	44% S(27) 19% S(21)
16	A”	924	2.73	0.22	0.75	37% S(44) 34% S(40)
17	A’	962	25.25	0.68	0.37	32% S(19) 16% S(1) 13% S(29) 11% S(15)
18	A”	985	1.48	5.53	0.75	35% S(52) 34% S(48)
19	A’	1037	0.82	11.49	0.75	66% S(26) 11% S(17)
20	A”	1073	0.13	3.43	0.75	22% S(43) 19% S(48) 15% S(52) 10% S(32)
21	A”	1090	0.00	0.35	0.75	84% S(47)
22	A’	1093	23.11	1.80	0.75	34% S(1) 27% S(29) 15% S(15)
23	A”	1100	0.01	3.18	0.75	33% S(39) 17% S(46) 16% S(42) 12% S(52)
24	A’	1174	6.98	5.35	0.12	22% S(15) 20% S(19) 10% S(24) 10% S(21)
25	A”	1201	0.18	3.19	0.75	31% S(43) 16% S(38) 10% S(48)
26	A’	1252	4.25	3.91	0.68	39% S(11) 20% S(18) 12% S(13)
27	A”	1289	1.24	2.47	0.75	39% S(46) 19% S(39) 12% S(32)
28	A’	1293	1.73	13.17	0.74	67% S(14)
29	A’	1312	0.04	2.23	0.59	50% S(18) 30% S(11)
30	A”	1336	0.01	5.38	0.75	39% S(38) 24% S(32) 12% S(43) 11% S(39)
31	A”	1362	0.03	2.50	0.75	34% S(42) 21% S(32) 13% S(45) 10% S(38)
32	A”	1367	0.01	0.72	0.75	25% S(42) 16% S(38) 15% S(39) 15% S(32)
33	A’	1378	0.60	0.47	0.62	41% S(17) 23% S(13)
34	A”	1379	0.02	2.16	0.75	54% S(45) 11% S(43)
35	A’	1389	2.24	1.90	0.69	48% S(13) 30% S(17)
36	A’	1413	1.71	4.11	0.38	82% S(22)
37	A”	1483	0.09	16.69	0.75	65% S(37) 31% S(41)
38	A’	1486	4.86	10.85	0.75	60% S(20) 35% S(12)
39	A”	1487	5.62	0.08	0.75	66% S(41) 32% S(37)
40	A’	1493	13.75	0.06	0.10	66% S(16) 25% S(12)
41	A’	1505	1.30	0.71	0.73	37% S(12) 31% S(20) 30% S(16)
42	A’	1794	267.96	23.39	0.44	91% S(10)
43	A’	2845	97.12	70.67	0.31	99% S(9)
44	A”	2997	17.15	7.90	0.75	70% S(34) 18% S(33)
45	A’	3001	20.96	14.03	0.68	63% S(4) 15% S(8) 14% S(3)
46	A’	3001	12.51	332.75	0.15	41% S(8) 16% S(7) 14% S(6) 13% S(5)
47	A”	3009	7.93	30.76	0.75	80% S(36) 11% S(34)
48	A’	3011	48.09	68.74	0.25	67% S(6) 23% S(8)
49	A’	3038	8.10	57.51	0.74	73% S(2) 14% S(3) 10% S(4)
50	A”	3052	85.78	4.47	0.75	60% S(35) 15% S(33) 13% S(36)
51	A’	3052	58.22	148.70	0.25	56% S(7) 18% S(8) 11% S(5) 10% S(6)
52	A”	3055	5.55	124.63	0.75	65% S(33) 25% S(35)
53	A’	3055	6.58	240.92	0.15	47% S(5) 20% S(3) 10% S(7)
54	A’	3062	103.84	48.90	0.00	42% S(3) 24% S(5) 16% S(2) 13% S(7)
axial-gauche (12.4%) E_{tot}=–349.116050 H						
1	A	80	6.00	1.49	0.75	69% S(54) 10% S(24) 10% S(31)
2	A	143	1.97	0.87	0.64	48% S(31) 11% S(24)
3	A	183	2.90	0.50	0.75	52% S(51) 19% S(53) 12% S(54)
4	A	272	2.03	0.76	0.19	27% S(31) 25% S(24)
5	A	318	4.25	0.61	0.51	34% S(53) 22% S(51) 10% S(23) 10% S(28)
6	A	376	0.15	0.47	0.70	58% S(28) 14% S(30)
7	A	424	1.28	1.00	0.74	74% S(50)
8	A	465	1.08	0.47	0.69	46% S(30) 13% S(29)
9	A	563	0.71	1.89	0.30	21% S(29) 16% S(23) 11% S(19)
10	A	663	1.63	3.56	0.10	16% S(24) 14% S(23) 12% S(1)
11	A	754	11.48	17.30	0.05	45% S(25) 13% S(27) 12% S(23)
12	A	792	0.12	1.27	0.65	41% S(44) 38% S(40) 13% S(48)
13	A	829	5.31	7.84	0.17	36% S(27) 34% S(25)
14	A	846	4.12	1.87	0.46	41% S(21) 25% S(15)

Table 6 (continued)

i	S_p	*k*	I	S	ρ	PED
15	A	874	2.44	0.54	0.75	71% S(49)
16	A	919	19.69	3.31	0.72	26% S(27) 21% S(1)
17	A	944	3.01	1.60	0.64	34% S(44) 30% S(40)
18	A	982	5.92	6.16	0.43	28% S(52) 13% S(1) 11% S(19)
19	A	1034	2.38	9.40	0.74	32% S(26) 23% S(29) 13% S(19)
20	A	1047	2.19	6.49	0.74	38% S(48) 11% S(32)
21	A	1054	0.40	1.39	0.74	23% S(26) 15% S(29)
22	A	1097	0.51	0.03	0.75	55% S(47) 16% S(39)
23	A	1131	0.22	0.35	0.74	18% S(32) 16% S(43) 16% S(42) 14% S(38) 12% S(39)
24	A	1146	0.25	1.85	0.37	20% S(15) 15% S(19) 13% S(52) 10% S(21)
25	A	1173	3.79	2.00	0.73	23% S(43) 18% S(47) 14% S(39)
26	A	1250	2.33	0.97	0.31	25% S(11) 19% S(14) 14% S(18) 10% S(19)
27	A	1283	0.38	11.23	0.75	33% S(46) 22% S(32) 11% S(48)
28	A	1297	0.62	15.14	0.75	55% S(18) 14% S(14)
29	A	1311	4.11	3.09	0.72	34% S(39) 15% S(32) 12% S(46)
30	A	1347	3.41	0.37	0.75	19% S(17) 17% S(11) 11% S(14)
31	A	1356	0.49	0.67	0.59	41% S(38) 20% S(42)
32	A	1374	0.05	0.17	0.28	40% S(42) 16% S(46) 11% S(43)
33	A	1379	0.94	0.62	0.71	40% S(45) 21% S(13)
34	A	1385	0.69	0.53	0.73	45% S(13) 15% S(45) 10% S(38)
35	A	1391	1.76	0.20	0.68	52% S(17) 26% S(14)
36	A	1416	2.03	4.35	0.46	80% S(22)
37	A	1481	4.61	14.03	0.75	73% S(37) 14% S(12)
38	A	1487	2.58	10.54	0.75	51% S(20) 25% S(12) 17% S(37)
39	A	1491	8.17	1.83	0.75	73% S(41) 13% S(16)
40	A	1497	12.47	0.84	0.75	36% S(12) 20% S(16) 19% S(20) 16% S(41)
41	A	1508	2.18	1.14	0.72	65% S(16) 15% S(12) 15% S(20)
42	A	1796	181.08	12.59	0.50	91% S(10)
43	A	2845	128.56	102.59	0.37	99% S(9)
44	A	2964	25.50	74.01	0.44	97% S(2)
45	A	2995	14.76	127.53	0.24	53% S(8) 19% S(7)
46	A	3003	30.91	22.50	0.67	33% S(36) 29% S(6) 24% S(8)
47	A	3013	26.36	39.24	0.62	84% S(34)
48	A	3018	41.23	171.55	0.09	79% S(4)
49	A	3026	17.95	152.94	0.22	47% S(36) 43% S(6)
50	A	3045	44.20	63.81	0.70	31% S(3) 28% S(33) 14% S(35)
51	A	3051	54.15	240.54	0.11	56% S(7) 19% S(8) 13% S(6)
52	A	3055	44.83	97.80	0.46	49% S(35) 16% S(33) 16% S(3)
53	A	3065	65.55	47.76	0.51	58% S(5) 22% S(35)
54	A	3079	24.25	89.64	0.30	39% S(3) 37% S(33)

1385 cm^{-1}. The CH out-of-plane bend is of A" symmetry in the *trans* conformer and appears highly mixed with other coordinates at 985 cm^{-1} with 35% S(52) in the *trans* form, and at 970 cm^{-1} with only 25% S(52) in *eg*. However, in both cases S(52) is the leading contribution to the corresponding fundamentals. It was not clearly assigned in the case of cyclobutanecarboxaldehyde. The in-plane CCO vibration was assigned to the Raman line observed at 577 cm^{-1} in the spectrum of liquid cyclobutanecarboxaldehyde. [3] This line shows up at different wavenumbers in the two conformers, because of the different type of mixing of symmetry coordinates in both of them. In *eg* it appears with 43% S(23) at 677 cm^{-1}, while in *et* there are 40% S(23) at 566 cm^{-1}. It must be noted that in *et* symmetry coordinates of A' do not mix with those of A" symmetry, while in *eg* they are all of A symmetry and thus can and actually, as in this case, do mix. The two ring-CO modes were assigned to lines observed at 335 cm^{-1} (polarized) and at 256 cm^{-1} (depolarized) in the Raman spectrum of liquid cyclobutanecarboxaldehyde. [3] The ring-CHO out-of-plane bend can be assigned to the line at 291 cm^{-1} [70% S(53)] in the *et* conformer, while due to strong mixing with other coordinates in the corresponding fundamentals it contributes to the lines at 215 cm^{-1} [31% S(53)] and 232 cm^{-1} [22% S(53)] in *eg*. The ring-CHO bend contributes to three modes in *et* and to four modes in *eg*. These are the fundamentals at 111 cm^{-1} [23% S(24)], 293 cm^{-1} [13% S(24)], and at 403 cm^{-1} [22% S(24)] in *et*, and at 71 cm^{-1} [16% S(24)], at 143 cm^{-1} [12% S(24)], at 316 cm^{-1} [20% S(24)], and at 412 cm^{-1} [10% S(24)] in *eg*. Thus a clear assignment of this motion to a single fundamental is not quite possible. The lowest fundamental in both conformers is dominated by the antisymmetric torsion of the CHO group [71 cm^{-1} with 68% S(54) in *eg*, 60 cm^{-1} with 82% S(54) in *et*]. The lowest skeletal modes should be due to the motion of the heavy atoms in the ring and, thus, should be the ring puckering [S(28), S(31)] and the ring twist [S(51)]. These motions contribute, with one exception, again to many fundamentals and thus it is once more impossible to assign a specific mode to these motions. Only in the *et* conformer can the ring

twist be assigned to the line at 220 cm^{-1} [91% S(51)]. In the *gauche* conformer this motion is the dominant participant in the two modes at 215 cm^{-1} and 232 cm^{-1} [35% S(51) and 51% S(51)] to which also the ring-CHO out-of-plane bend [S(53)] contributes strongly.

Thus, it is obvious that in such a large molecule quite a few symmetry coordinates must be used to describe some of the normal modes and in most cases it is not possible to assign just one mode to one symmetry coordinate. However, the PED values in Table 6 give insight into the degree of mixing of symmetry coordinates in the different modes and thus into the nuclear motions belonging to each vibration. As next step we have to calculate and plot the spectra from the data obtained and compare the result to the experimental spectrum.

Vibrational infrared and Raman spectra

For the infrared spectrum we used the intensities I_j as given by the DFT calculations (all relative to the largest one in the conformers present in the mixture at 300 K) and converted them to relative transmittances. In the case of the Raman spectra, we used the scattering activities S_j, the wavenumbers k_j, and the depolarization ratios ρ_j for each normal mode j as calculated in the DFT runs for the conformers. Then the Raman cross sections which are proportional to the intensities are given as [15, 23]

$$\frac{\partial\sigma_j}{\partial\Omega} = \frac{2^4\pi^4}{45}\frac{h(k_o-k_j)^4}{8\pi^2 c k_j\left[1-e^{-\frac{hck_j}{k_B T}}\right]} S_j \frac{1-\rho_j}{1+\rho_j} \tag{1}$$

Since we are interested only in relative intensities, we calculated them as

$$I_j = \frac{\frac{\partial\sigma_j}{\partial\Omega}}{\frac{\partial\sigma_{j_m}}{\partial\Omega}} \tag{2}$$

where j_m denotes that line among all the lines from all conformers present in the mixture that has the largest Raman cross section. As laser wavelength we used that of an argon ion laser at λ_o=514.5 nm (k_o=1/λ_o). As temperature we used T=300 K. Then the line shapes are calculated as Lorentzians (L) with a width of $\Delta\nu$=15 cm^{-1} corresponding to the estimated average width in the experimental spectrum used for comparison. Thus the final spectrum for one conformer is calculated as

$$I(k) = \sum_j I_j L(k-k_j)L(k-k_j) = \frac{1}{\pi}\frac{\frac{\Delta k}{2}}{(k-k_j)^2+\left(\frac{\Delta k}{2}\right)^2}\int_{-\infty}^{\infty} L(k-k_j)\mathrm{d}k = 1 \tag{3}$$

where the index j runs over all normal modes. For the plots a step size for the grid of generally 10 cm^{-1} was used. However, when a line appears between two consecutive grid points, 12 extra points with a step size of 0.5 cm^{-1} are inserted into this interval, which includes the exact center of the line.

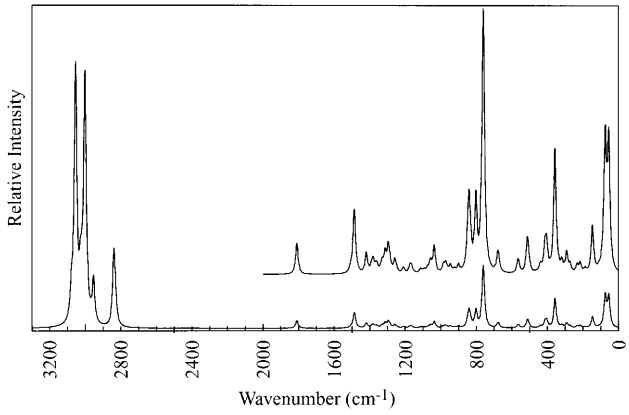

Fig. 3 Calculated vibrational Raman spectrum of a mixture containing 63.3% *eg*, 24.3% *et* and 12.4% *ag* conformer (line width is 15 cm^{-1})

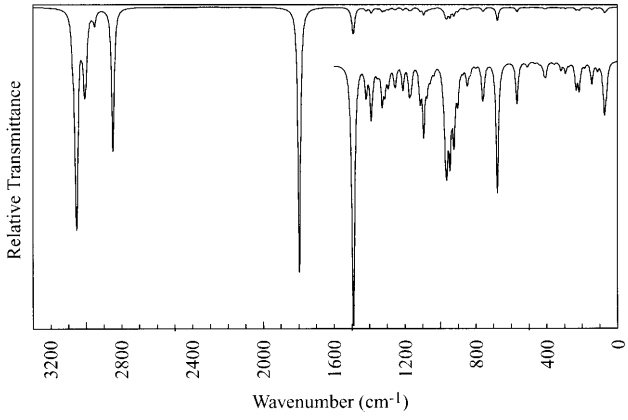

Fig. 4 Calculated vibrational infrared spectrum of a mixture containing 63.3% *eg*, 24.3% *et* and 12.4% *ag* conformer (line width is 15 cm^{-1})

After calculation of the spectra of all conformers, they are superimposed with the help of the Boltzmann distribution. Then the total intensity as function of wavenumber for a mixture of N+1 different conformers is given by

$$I(k) = \frac{\sum_{l=0}^{N} g_l I_l(k)\, e^{-\frac{\Delta E_l}{k_B T}}}{\sum_{l=0}^{N} g_l\, e^{-\frac{\Delta E_l}{k_B T}}} \tag{4}$$

Here $I_l(k)$ are the individual spectra of the conformers, l=0 corresponds to the most stable conformer, ΔE=E_l–E_0 is the energy of each conformer relative to the most stable one, E_l is the absolute total energy of conformer l and g_l is the degeneracy of conformer l (in our case 2 for *gauche* conformers and 1 for *et*).

In Figs. 3 and 4 we show the calculated Raman and infrared spectra, respectively. The insets are in each case magnified plots of the underlying low relative intensity and transmittance parts of the corresponding spectra. A detailed inspection of the spectra and comparison with

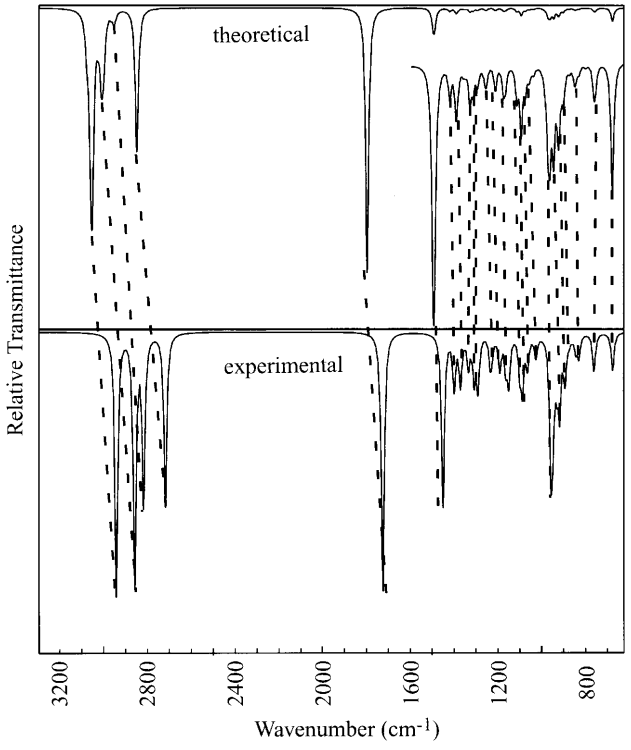

Fig. 5 Calculated vibrational infrared spectrum of a mixture containing 63.3% *eg*, 24.3% *et* and 12.4% *ag* conformer in comparison to a replotted experimental one (line width is 15 cm^{-1})

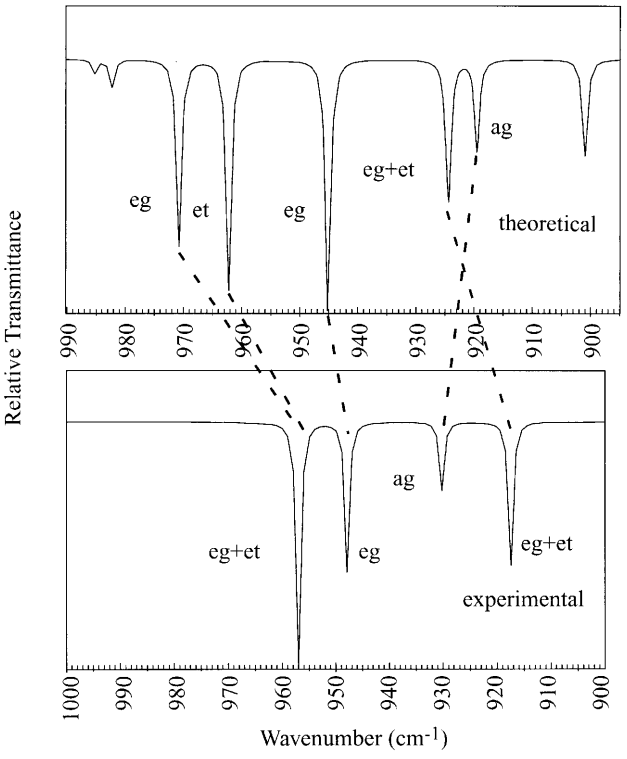

Fig. 6 Calculated vibrational infrared spectrum of a mixture containing 63.3% *eg*, 24.3% *et* and 12.4% *ag* conformer in comparison to a replotted experimental one between about 900 cm^{-1} and about 1000 cm^{-1}, with a line width of 1 cm^{-1}

Table 6 reveals that there are no lines whose presence or absence in an experimental spectrum could help to reach a conclusion whether or not the *ag* conformer is present in a mixture of conformers. Also, the overall appearance of the spectrum has no distinctive features that would tell us about the abundances of the conformers. This is more clearly seen in Fig. 5 where we plot the theoretical infrared spectrum in comparison to a replot of an experimental one from the Aldrich library. [24] We have measured the peak line intensities in that spectrum together with the wavenumbers and replotted it with a common line width of 15 cm^{-1} in the same way as the theoretical ones. When assuming a common average line width, relative peak intensities are proportional to relative integrated intensities (Equation 3). It is clear that in the region below 1600 cm^{-1} the overall agreement between the two spectra is rather good and no conclusion can be drawn whether *ag* is present or not in the experimental spectrum. However, it is clear from the previous discussion that, due to the problems with total energy differences in our calculations, this is a crucial open question, because the spectra depend via the abundances on total energy differences, while the spectra of the individual conformers do not.

Therefore, we concentrate on a small region of the spectra, roughly between 900 cm^{-1} and 1000 cm^{-1}, where a distinctive feature can be seen in Fig. 5. Figure 6 shows plots of this region with line widths of 1 cm^{-1}. We see that here the theoretical spectrum contains five lines corresponding to the four lines in the experimental spectrum. The theoretical line at 900 cm^{-1} belongs to a line below that wavenumber in the experimental spectrum. To explain the large intensity of the experimental line at roughly 957 cm^{-1} we have to assume that the two lines, one from *eg* and one from *et*, in the theoretical spectrum are seen as one line in the experimental one. Further, we have to assume that the *ag* wavenumber in the theoretical spectrum is somewhat underestimated. In contrast to HF or MP2, which almost always overestimate wavenumbers, DFT is known to both over- and underestimate terms, depending on the line under consideration. [12] Since the functional form of the theoretical spectrum is known analytically together with the intensities of each line in each conformer, this can be used to determine an estimate as to how much intensity at a peak wavenumber actually is due to the line peak there itself and how much is contributed from neighboring lines. Assigning in this way the relative intensity of the strongest experimental line to 1, we get a sequence of effective relative intensities in the experimental spectrum of 1.00, 0.64, 0.24, and 0.49 with decreasing wavenumber. Two of these lines are assigned to only one conformer, and the strongest one to *eg+et*. Thus we can estimate by forming ratios of intensities and using the theoretical intensities from Table 6 the abundances which would correspond to the

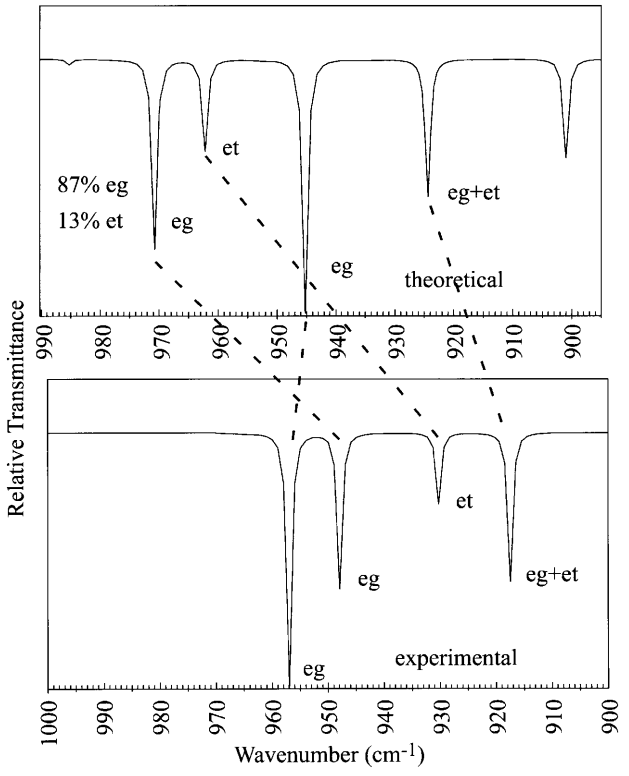

Fig. 7 Calculated vibrational infrared spectrum of a mixture containing 87% *eg* and 13% *et* conformer in comparison to a replotted experimental one between about 900 cm- and about 1000 cm^{-1}, with a line width of 1 cm^{-1}

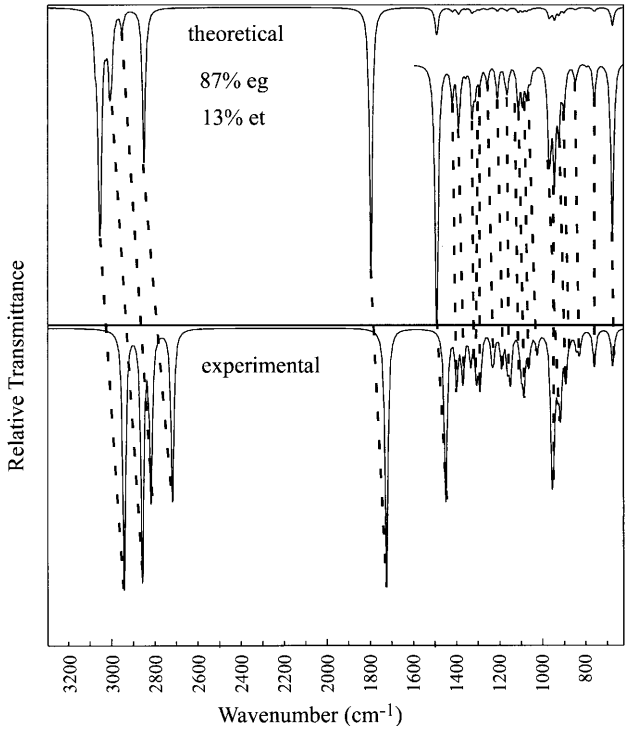

Fig. 8 Calculated vibrational infrared spectrum of a mixture containing 87% *eg* and 13% *et* conformer in comparison to a replotted experimental one (line width is 15 cm^{-1})

experimental lines, provided that our assignment (not sure) and the theoretical intensities (qualitatively correct) are correct:

$$\frac{1}{0.64} = \frac{7.85\,eg + 25.25\,et}{10.49\,eg} \rightarrow 1.563 = 0.748 + 2.407\frac{et}{eg}$$
$$\rightarrow \frac{et}{eg} = 0.339\ (theoretical:\ 0.384)$$
$$\frac{0.24}{0.64} = \frac{19.69\,ag}{10.49\,eg} \rightarrow \frac{ag}{eg} = 0.200\ (theoretical:\ 0.196) \quad (5)$$
$$\frac{0.49}{0.64} = \frac{5.48\,eg + 2.73\,et}{10.49\,eg} \rightarrow 0.766 = 0.522 + 0.260\frac{et}{eg}$$
$$\rightarrow \frac{et}{eg} = 0.938$$

Obviously the first two intensity ratios give abundance ratios in excellent agreement with the ratios from our DFT calculations. Unfortunately, as the last example shows, other ratios yield results completely inconsistent with DFT data. Note that other assignments of the lines we tried yield results that are even more inconsistent with respect to each other and with respect to the DFT results, some even giving negative abundances.

Thus we reach the same conclusion as before: While results based on total energy derivatives such as geometries, wavenumbers, and intensities derived from the DFT data can be trusted, total energy differences cannot. Thus in Fig. 7 we show the same type of plot as in Fig. 6, but now the abundances on which the theoretical spectrum is based are the experimental ones. [10] Assuming that the wavenumber of the most intense theoretical line is underestimated by roughly 10 cm^{-1}, we obtain a nearly one to one correspondence between theoretical and experimental spectra. Therefore, we conclude that the experimental abundances of conformers are the correct ones (it could have been possible that a 12% *ag* contribution might have been overlooked in the microwave spectrum). Thus Fig. 8 shows again the comparison of the complete spectra, the theoretical one now calculated with a mixture of 87% *eg* and 13% *et*. Figures 9 and 10 show the Raman and infrared spectra in total for these abundances. The overall agreement in the lower wavenumber part is of roughly the same quality as in Fig. 5, but with some details improved. There are two problems at the extreme ends of the spectrum. The relative intensity of the lowest wavenumber line seems to be far too high in the theoretical spectrum. However, for the corresponding experimental line, it was difficult to obtain the intensity, because this line is a rather broad feature, superimposed on a very high background noise. Thus, we might have severely underestimated its intensity from the experimental spectrum.

The other problem lies at the opposite end of the spectra. The intensities of the CH stretches and of the CO stretch are strongly overestimated, also relative to

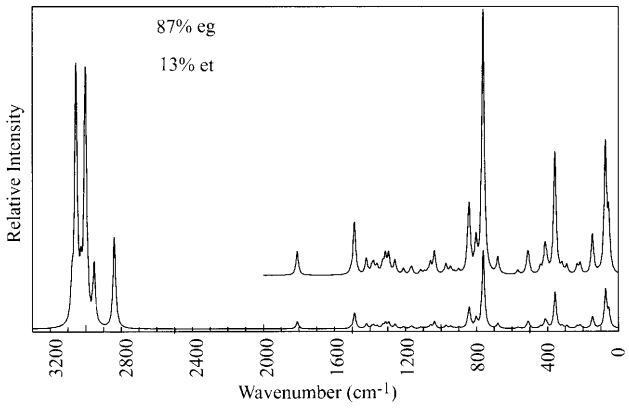

Fig. 9 Calculated vibrational Raman spectrum of a mixture containing 87% *eg* and 13% *et* conformer (line width is 15 cm^{-1})

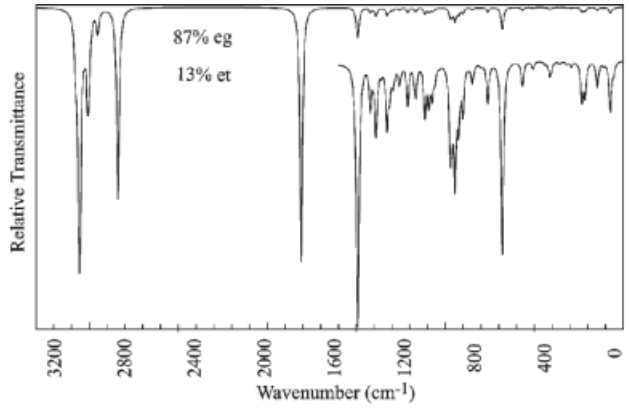

Fig. 10 Calculated vibrational infrared spectrum of a mixture containing 87% *eg* and 13% *et* conformer (line width is 15 cm^{-1})

each other, while the wavenumbers are more in error in DFT than for the lines below 1600 cm^{-1}. In the case of the CH stretches, the reasons are utterly clear and textbook knowledge: theoretical CH stretches suffer notoriously from anharmonicities in the experimental potential curves. Since in anharmonic potentials other wavefunctions have to be used, intensities calculated in the harmonic approximation as done here can also be quite wrong for these vibrations. Figure 11a shows a potential scan of the $C–H_{ald}$ stretch as an example, starting from the *eg* minimum geometry. The dashed line is plotted from a parabola, centered at the equilibrium bond length and with the force constant given by the DFT calculation for this mode, which is composed to 99% from the $C–H_{ald}$ stretch. The anharmonic contributions to the scanned potential function (single point DFT calculation at different bond lengths) as compared to the harmonic parabola are clearly visible, even around the minimum. Figure 11b shows the potentials for the CO stretch. Clearly, in this case the deviations from a harmonic potential are even larger than in the well-known CH case. Thus the CO stretch suffers from the same troubles as the CH stretches, a trouble which cannot be removed by simply increasing basis set sizes, quality of DFT functionals (as most functionals B3LYP suffers from an artificial electron self-interaction contribution), or correlation levels.

Conclusion

In conclusion, our DFT calculations have provided us, apart from deficiencies in absolute values of total energies due to basis set problems, with rather reliable information about the geometries of the stable conformers of cyclohexanecarboxaldehyde. The basis set problems are difficult to avoid when large atomic basis sets are used in

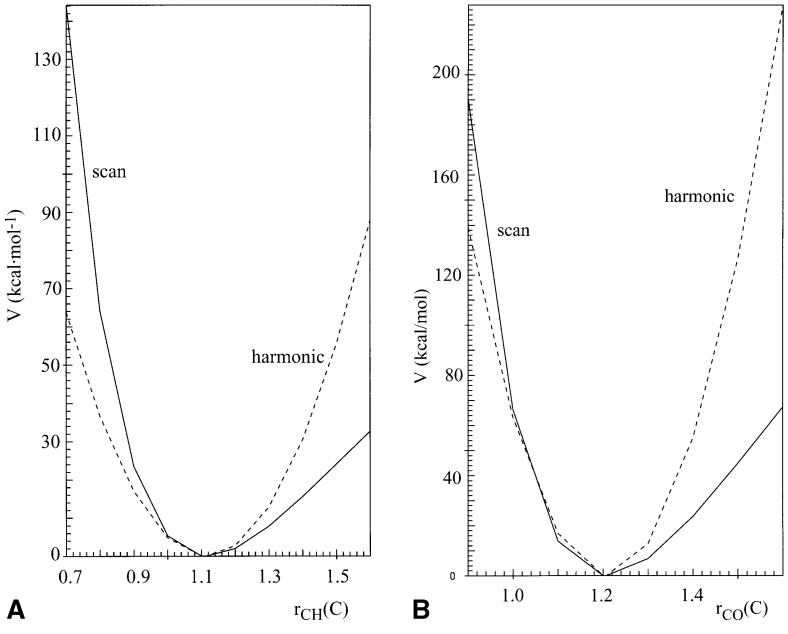

Fig. 11a,b Potentials *V* relative to their minimal values as functions of the respective bond lengths as obtained from a DFT potential scan (solid line) and from a parabola centered at the equilibrium bond length, $V(r)=(1/2)f(r–r_o)^2$ (dashed line), having a force constant *f* as given in the Gaussian output for the respective modes (*eg* conformer as equilibrium) for **a** $C–H_{ald}$ bond stretch and **b** C=O bond stretch

molecules containing a comparatively large number of atoms. Smaller atomic basis sets, on the other hand, could render other properties than total energies unreliable. According to our comparisons to experiment, all properties based on derivatives of the total energy are obtained in fair agreement with experimental data, even shapes of spectra. In the latter case one should keep in mind that only the lower wavenumber parts of the spectra are represented well, while CH and CO stretches suffer from anharmonicities. The relative stability of conformers does not agree with experiment, because they are based on differences of numbers of the order Gcal mol^{-1}, resulting in numbers of the order of kcal mol^{-1}. Thus the basis set problems play a role here. They do not in the calculation of derivatives, which can be done analytically not as differences of large numbers (containing relatively small errors). The vibrational assignments of normal modes of large molecules like ours are not always straightforward, because in many cases several symmetry coordinates can participate in one normal mode. However, explicitly given PED values give insight into the degree of mixing of different atomic movements in a normal mode. The Cartesian coordinates of the three stable conformers are available as Supplementary Material to this article.

Acknowledgement The authors gratefully acknowledge the support of this work by King Fahd University of Petroleum and Minerals through the Grant CY/VIBRATION/194. We thank Dr. Wenym Y. Zhao for providing the symmetry coordinates of fluorocyclohexane as model system.

Appendix

To start our PED calculations, we read from the Gaussian98 output the normal mode wavenumbers k_k in cm^{-1} and the coefficients N_x in Cartesian coordinates. Because we have to take some precautions due to the fact that these coefficients are given only to an accuracy of two digits after the decimal point, we outline our procedures here in some detail, although they are based on the considerations given in Wilson's book. [14] First of all, to arrive at a consistent system of units with masses in amu, lengths in Å, and force constants in mdyne Å^{-1}, we calculate

$$\varepsilon_k = \left(\frac{k_k}{\sqrt{f_k / m_k^*}}\right)^2 = \left(\frac{k_k}{1302.78}\right)^2 \tag{A1}$$

where f_k is the force constant, m_k^* the effective mass and k_k the wavenumber in cm^{-1} of normal mode k. Note that singly underlined quantities are column vectors, while doubly underlined ones are matrices. The vector of normal coordinates is then

$$\underline{n} = \underline{\underline{N}}_x^+ \underline{x} \tag{A2}$$

where the dagger denotes (for our real matrices here) the transpose of a matrix. $\underline{x}$ is a vector containing the $3N$ (N is the number of atoms) Cartesian displacements (3 for each atom) from equilibrium. N_x is thus a $3N\times(3N–6)$ matrix, because translations and rotations are not included so far. Therefore:

$$n_k = \sum_i (\underline{\underline{N}}_x^+)_{ki} x_i = \sum_i (\underline{\underline{N}}_x)_{ik} x_i \tag{A3}$$

As a next step because of the inaccuracies of the normal mode coefficients we normalize and orthogonalize them with respect to an "overlap" matrix M, containing the atomic masses on its diagonal and 0 otherwise. Each mass has to appear three times in sequence because of the three Cartesian displacements for each atom. This orthonormalization corresponds to the fact that the mass-weighted Cartesian normal mode coefficients N_q have to be orthonormal with metric 1:

$$\begin{aligned} &\underline{n} = \underline{\underline{N}}_x^+ \underline{x} = \underline{\underline{N}}_q^+ \underline{q}; \underline{q} = \underline{\underline{M}}^{-1/2} \underline{x} \\ &\underline{\underline{N}}_q = \underline{\underline{M}}^{1/2} \underline{\underline{N}}_x; \underline{\underline{N}}_q^+ \underline{\underline{N}}_q = \underline{\underline{1}} \\ &\quad \underline{\underline{N}}_x^+ \underline{\underline{M}} \underline{\underline{N}}_x = \underline{\underline{1}} \end{aligned} \tag{A4}$$

The force constant matrix F_q in mass weighted Cartesian coordinates can be derived from the fact that the potential energy V does not depend on the coordinate system:

$$\begin{aligned} &2V = \underline{x}^+ \underline{\underline{F}}_x \underline{x} = \underline{q}^+ \underline{\underline{M}}^{-1/2} \underline{\underline{F}}_x \underline{\underline{M}}^{-1/2} \underline{q} = \underline{q}^+ \underline{\underline{F}}_q \underline{q} \\ &\underline{\underline{F}}_q = \underline{\underline{M}}^{-1/2} \underline{\underline{F}}_x \underline{\underline{M}}^{-1/2}; \underline{n} = \underline{\underline{N}}_q^+ \underline{q}; \underline{\underline{F}}_q \underline{\underline{N}}_q = \underline{\underline{N}}_q \underline{\underline{\varepsilon}}; \varepsilon_{k'k} = \varepsilon_k \delta_{k'k} \end{aligned} \tag{A5}$$

Thus from our input data we can construct F_q:

$$\underline{\underline{F}}_q = \underline{\underline{N}}_q \underline{\underline{\varepsilon}} \underline{\underline{N}}_q^+ \tag{A6}$$

In all further calculations we do not use the normal mode coefficients read in, but those obtained by diagonalization of the so formed F_q. This yields the same eigenvalues ε_k, but somewhat more accurate coefficients N_q. Note that this matrix now contains also rotations and translations and is therefore a square matrix of dimension $3N\times3N$.

To obtain a PED, we now have to transform force constant matrices and normal mode coefficients first into a space of internal coordinates and then into one of symmetry coordinates. The latter define the atomic motions that one would like to assign the normal modes to, while the former ones are introduced just to make it easier to define the latter. For a complete description of all possible internal motions one needs at least a complete set of independent internal coordinates ($3N$–6). Anyone of them can be built from the 5 primitive ones: bond stretch, bond angle bend, wag, torsion, and libration. The latter are only needed if parts of the molecule are linear (at least 3 collinear atoms). The program input just defines what type of internal coordinate is desired together with the numbers of the atoms involved. Then following [14] and using the equilibrium geometry of the molecule which is also part of the input, the program calculates the matrix B which links the inter-

nal coordinate vector $\underline{b}$ to the Cartesian displacement vector $\underline{x}$:

$$\underline{b} = \underline{\underline{B}}\underline{x}; b_j = \sum_i B_{ji} x_i \tag{7}$$

The user is free to introduce an overcomplete set of internal coordinates, since this usually makes the construction of the necessary symmetry coordinates easier. The complete set of independent internal coordinates would give a B of dimension $(3N–6)\times 3N$, a rectangular matrix, which has no normal inverse.

The next step in the input has to provide at least $3N–6$ coefficients which link the desired symmetry coordinate vector $\underline{s}$ to the internal coordinate vector $\underline{b}$. The coefficient matrix has to contain only orthogonal symmetry coordinates:

$$\underline{s} = \underline{\underline{U}}\underline{b} \tag{A8}$$

At this point there are two possibilities for the user. One can provide either a complete set of $3N–6$ symmetry coordinates together with six orthogonal redundant coordinates, or the user can provide only the $3N–6$ necessary orthogonal symmetry coordinates. The program detects which case is present and deals with it accordingly.

However, now as next step redundant internal coordinates must be identified and removed from the list of internal coordinates, as well as from matrix U which links symmetry and internal coordinates. This can be done by forming a square symmetric matrix BB^+. We use for inversions the fact that, for symmetric square matrices A, their inverse can be constructed from their eigenvalue λ (contains the eigenvalues on the diagonal and 0 else) and eigenvector matrices V:

$$\underline{\underline{A}}^{-1} = \underline{\underline{V}}\,\underline{\underline{\lambda}}^{-1}\,\underline{\underline{V}}^{+}; (\underline{\underline{\lambda}}^{-1})_{j'j} = \lambda_j^{-1}\delta_{j'j} \tag{A9}$$

We first diagonalize BB^+:

$$\underline{\underline{B}}(\underline{\underline{B}}^{+})\underline{\underline{V}} = \underline{\underline{V}}\underline{\underline{\lambda}}; \lambda_{j'j} = \lambda_j \delta_{j'j}; \underline{\underline{V}}\,\underline{\underline{V}}^{+} = \underline{\underline{V}}^{+}\underline{\underline{V}} = \underline{\underline{1}} \tag{A10}$$

Then we have a redundant internal coordinate for each zero eigenvalue of this matrix. The eigenvalues we can get by

$$\underline{\underline{V}}^{+}\,\underline{\underline{B}}\,\underline{\underline{B}}^{+}\,\underline{\underline{V}} = \underline{\underline{\lambda}} \tag{A11}$$

Therefore an eigenvalue of zero with index say j_o means:

$$\sum_{k'k} V_{kj_o}(\underline{\underline{B}}\,\underline{\underline{B}}^{+})_{k'k} V_{k'j_o} = \lambda_{j_o} = 0 \Rightarrow \sum_l \left(\sum_k V_{kj_o} B_{kl}\right)^2 = 0 \Rightarrow \sum_k V_{kj_o} B_{kl} = 0 \tag{A12}$$

The existence of a relation like the latter between internal coordinates just proves linear dependence. To choose an internal coordinate with index k_o to be removed from the matrix B, the program chooses k_o such that

$$|V_{k_o j_o}| = max|V_{kj_o}| \tag{A13}$$

If after removal of an internal coordinate for each zero eigenvalue of BB^+, there are $3N–6$ independent coordinates left, the program goes on with the calculation. If the set is not complete, it indicates the fact in the output and stops execution. Redundants must be removed because BB^+ cannot be inverted if it has zero eigenvalues.

However, now the deleted dependent coordinates have to be removed from U also. Assume an internal coordinate k_o has to be removed. Then from the above discussion we have the equation

$$B_{k_o l} = -\sum_{k\neq k'} \frac{V_{kj_o}}{V_{k_o j_o}} B_{kl} \tag{A14}$$

Let us call the matrix still containing the redundant internal coordinate U', and the new one obtained after removal U:

$$\begin{aligned} s_n &= \sum_k U'_{nk} b_k = \sum_k U'_{nk} \sum_l B_{kl} x_l \\ &= \sum_l \left[\sum_{k\neq k_o} U'_{nk} B_{kl} + U'_{nk_o} B_{k_o l}\right] x_l \\ &= \sum_l \left[\sum_{k\neq k_o} U'_{nk} B_{kl} - U'_{nk_o} \sum_{k\neq k_o} \frac{V_{kj_o}}{V_{k_o j_o}} B_{kl}\right] x_l \end{aligned} \tag{A15}$$

In the last line of equation (A15) we just have inserted equation (A14). From this we get our new symmetry coordinate matrix as:

$$\begin{aligned} s_n &= \sum_{k\neq k_o} \left[U'_{nk} - U'_{nk_o} \frac{V_{kj_o}}{V_{k_o j_o}}\right] \sum_l B_{kl} x_l \\ &= \sum_{k\neq k_o} \left[U'_{nk} - U'_{nk_o} \frac{V_{kj_o}}{V_{k_o j_o}}\right] b_k \\ U_{nk} &= U'_{nk} - \frac{V_{kj_o}}{V_{k_o j_o}} U'_{nk_o} \end{aligned} \tag{A16}$$

As next step the program orthogonalizes the old internal coordinates (let us call the old matrix B' from now on, and the new one B) to the translations and rotations contained in N_q as obtained from diagonalization of F_q. This is again necessary because of the low accuracy of the N_x input. Let us call the $6\times 3N$ matrix, which links the translations and rotations to the Cartesian displacements, T. Then our new B matrix has to fulfill

$$\sum_l B_{kl} T_{jl} = 0 \tag{A17}$$

where index j runs from 1 to 6. This is reached by adding a linear combination of the translations and rotations with yet unknown coefficients α to the old matrix B':

$$\begin{aligned} B_{kl} &= B'_{kl} + \sum_{j=1}^{6} \alpha_{kj} T_{jl} \\ &\Rightarrow \sum_l \left[B'_{kl} + \sum_{j=1}^{6} \alpha_{kj} T_{jl}\right] T_{j'l} = 0 \end{aligned} \tag{A18}$$

With the following definitions ($N(T)_q$ denotes that part of N_q which describes the six translations and rotations)

$$\begin{aligned} \underline{\underline{X}} &\equiv \underline{\underline{T}}\,\underline{\underline{T}}^{+} = \underline{\underline{N}}(T)_q^{+}\,\underline{\underline{M}}^{-1}\,\underline{\underline{N}}(T)_q \\ \underline{\underline{a}} &\equiv \underline{\underline{B}}'\,\underline{\underline{T}}^{+};\ \underline{\underline{T}} \equiv \underline{\underline{M}}^{-1/2}\,\underline{\underline{N}}(T)_q \end{aligned} \tag{A19}$$

we obtain

$$\underline{\underline{a}} = -\underline{\underline{\alpha X}} \tag{A20}$$

Since X is a square but not a symmetric matrix our program cannot invert it. Thus:

$$\begin{aligned} \underline{\underline{a}}\,\underline{\underline{X}}^{+} &= -\underline{\underline{\alpha X}}\,\underline{\underline{X}}^{+} \\ \underline{\underline{\alpha}} &= -\underline{\underline{a}}\,\underline{\underline{X}}^{+}\,(\underline{\underline{X}}\,\underline{\underline{X}}^{+})^{-1} \end{aligned} \tag{A21}$$

Note that XX^{+} is a symmetric square matrix. Thus our new B matrix is

$$\underline{\underline{B}} = \underline{\underline{B}}' - \underline{\underline{a}}\,\underline{\underline{X}}^{+}\,(\underline{\underline{X}}\,\underline{\underline{X}}^{+})^{-1}\,\underline{\underline{T}} \tag{A22}$$

Now the program adds the translations and rotations to B, to get a square matrix. However, note that the procedures outlined in the following work equally well for square unsymmetric as for rectangular matrices. If B is increased to a $3N\times 3N$ matrix, the same has to be done for the symmetry coordinate matrix U. This implies simply that for each translation or rotation in B one has to add a symmetry coordinate in U, which has as its only component just the internal translation or rotation coordinate under consideration.

Now we have to compute a force constant matrix in internal coordinates, F_b. To this end, a look at the potential energy V again shows the way:

$$\begin{aligned} 2V &= \underline{x}^{+}\,\underline{\underline{F}}_x\,\underline{x} = \underline{q}^{+}\,\underline{\underline{F}}_q\,\underline{q} = \underline{n}^{+}\,\underline{\underline{\varepsilon}}\,\underline{n} = \underline{b}^{+}\,\underline{\underline{F}}_b\,\underline{b} \\ &= \underline{x}^{+}\,\underline{\underline{B}}^{+}\,\underline{\underline{F}}_b\,\underline{\underline{B}}\,\underline{x} \Rightarrow \underline{\underline{F}}_x = \underline{\underline{B}}^{+}\,\underline{\underline{F}}_b\,\underline{\underline{B}} \end{aligned} \tag{A23}$$

With B being either rectangular or not invertible with our program, we have to resort to a trick:

$$\begin{aligned} \underline{\underline{B}}\,\underline{\underline{F}}_x\,\underline{\underline{B}}^{+} &= (\underline{\underline{B}}\,\underline{\underline{B}}^{+})\,\underline{\underline{F}}_b\,(\underline{\underline{B}}\,\underline{\underline{B}}^{+}) \\ \underline{\underline{F}}_b &= (\underline{\underline{B}}\,\underline{\underline{B}}^{+})^{-1}\,\underline{\underline{B}}\,\underline{\underline{F}}_x\,\underline{\underline{B}}^{+}\,(\underline{\underline{B}}\,\underline{\underline{B}}^{+})^{-1} \equiv \underline{\underline{A}}\,\underline{\underline{F}}_x\,\underline{\underline{A}}^{+} \\ \underline{\underline{A}} &\equiv (\underline{\underline{B}}\,\underline{\underline{B}}^{+})^{-1}\,\underline{\underline{B}} \end{aligned} \tag{A24}$$

In this way it is easy to calculate F_b from F_x for any form of B. A similar procedure we have when transforming F_b to F_s, with the force constant matrix in symmetry coordinates:

$$\begin{aligned} 2V &= \underline{s}^{+}\,\underline{\underline{F}}_s\,\underline{s} = \underline{b}^{+}\,\underline{\underline{U}}^{+}\,\underline{\underline{F}}_s\,\underline{\underline{U}}\,\underline{b} \\ &= \underline{b}^{+}\,\underline{\underline{F}}_b\,\underline{b} \Rightarrow \underline{\underline{U}}^{+}\,\underline{\underline{F}}_s\,\underline{\underline{U}} = \underline{\underline{F}}_b \end{aligned} \tag{A25}$$

From this we can calculate F_s from F_b in the same way as above. However, in almost all cases we use our program for, U is a square orthogonal matrix, i.e. $U^{-1} = U^{+}$. In this case we simply have $F_s = UF_bU^{+}$.

With $\underline{b} = N_b\underline{n}$ and $\underline{s} = N_s\underline{n}$, it is easy to show that

$$\begin{aligned} \underline{\underline{N}}_b &= \underline{\underline{B}}\,\underline{\underline{M}}^{-1/2}\,\underline{\underline{N}}_q = \underline{\underline{B}}\,\underline{\underline{N}}_x \\ \underline{\underline{N}}_s &= \underline{\underline{U}}\,\underline{\underline{B}}\,\underline{\underline{M}}^{-1/2}\,\underline{\underline{N}}_q = \underline{\underline{U}}\,\underline{\underline{B}}\,\underline{\underline{N}}_x \end{aligned} \tag{A26}$$

Thus we arrive at

$$\underline{\underline{\varepsilon}} = \underline{\underline{N}}_q^{+}\,\underline{\underline{F}}_q\,\underline{\underline{N}}_q = \underline{\underline{N}}_s^{+}\,\underline{\underline{F}}_s\,\underline{\underline{N}}_s \tag{A27}$$

Therefore the potential energy in the normal mode j, ε_j, is

$$\begin{aligned} \varepsilon_j &= (\underline{\underline{N}}_s^{+}\,\underline{\underline{F}}_s\,\underline{\underline{N}}_s)_{jj} = \sum_k (\underline{\underline{N}}_s^{+})_{jk}\,(\underline{\underline{F}}_s\,\underline{\underline{N}}_s)_{kj} \\ &= \sum_k (\underline{\underline{N}}_s)_{kj}\,(\underline{\underline{F}}_s\,\underline{\underline{N}}_s)_{kj} \end{aligned} \tag{A28}$$

And finally the contribution of the symmetry coordinate k to the potential energy of normal mode j, ε_j, in percent, PED_{kj}, is given by

$$\mathrm{PED}_{kj} = \frac{(\underline{\underline{N}}_s)_{kj}\sum_l (\underline{\underline{F}}_s)_{kl}\,(\underline{\underline{N}}_s)_{lj}}{\varepsilon_j} \times 100\% \tag{A29}$$

It is easy to see that the sum over all symmetry coordinates k yields 100% as required. However, due to the presence of negative coupling constants in F_s and F_b, small negative percentages can occur due to the inaccuracies in the N_x input. Further, if two coordinates are very strongly coupled, i.e. nearly linear dependent, even percentages larger than 100% for one of them compensated by percentages less than –100% for the other can occur. In such a case one has to change either internal or symmetry coordinates, to reduce coupling constants.

References

1. Durig, J. R.; Badawi, H. M.; Little, T. S.; Bist, H. D. *J. Chem. Phys.* **1986**, *85*, 5446.
2. Durig, J. R.; Badawi, H. M.; Bist, H. D.; Little, T. S. *J. Mol. Struct.* **1988**, *190*, 475.
3. Durig, J. R.; Badawi, H. M. *Chem. Phys.* **1990**, *148*, 193.
4. Badawi, H. M. *J. Mol. Struct.* **1990**, *205*, 353.
5. Badawi, H. M. *J. Mol. Struct.* **1990**, *208*, 7.
6. Badawi, H. M. *J. Mol. Struct.* **1991**, *228*, 159.
7. Badawi, H. M. *J. Mol. Struct.* **1996**, *369*, 75.
8. Badawi, H. M. Förner, W.; Al-Rayyes, A. J. *J. Mol. Model.* **1998**, *4*, 158.
9. Badawi, H. M. Förner, W. *J. Raman Spectrosc.* **1998**, *29*, 1009.
10. Kao, P. N.; Turner, P. H. *J. Am. Chem. Soc.* **1979**, *101*, 4997.
11. Gaussian 98, Revision A.7, Frisch, M. J.; Trucks, G. W.; Schlegel, H. B.; Scuseria, G. E.; Robb, M. A.; Cheeseman, J. R.; Zakrzewski, V. G.; Montgomery, Jr., J. A.; Stratmann, R. E.; Burant, J. C.; Dapprich, S.; Millam, J. M.; Daniels, A. D.; Kudin, K. N.; Strain, M. C.; Farkas, O.; Tomasi, J.; Barone, V.; Cossi, M.; Cammi, R.; Mennucci, B.; Pomelli, C.; Adamo, C.; Clifford, S; Ochterski, J.; Petersson, G. A.; Ayala, P. Y.; Cui, Q.; Morokuma, K.; Malick, D. K.; Rabuck, A. D.; Raghavachari, K.; Foresman, J. B.; Cioslowski, J.; Ortiz, J. V.; Baboul, A. G.; Stefanov, B. B.; Liu, G.; Liashenko, A.; Piskorz, P.; Komaromi, I.; Gomperts, R.; Martin, R. L; Fox, D. J.; Keith, T.; Al–Laham, M. A.; Peng, C. Y.; Nanayakkara, A.; Gonzalez, C.; Challacombe, M.; Gill, P. M. W.; Johnson, B.; Chen, W.; Wong, M. W.; Andres, J. L.; Gonzalez, C.; Head–Gordon, M.; Re-plogle, E. S., Pople, J. A.; Gaussian, Inc., Pittsburgh Pa., 1998.
12. Handy, N. C. In *Lecture Notes in Quantum Chemistry II*; Roos, B. O., Ed.; Springer Verlag: Berlin, Heidelberg, New York, 1994; p 91.
13. Badawi, H. M.; Förner, W. *Asian J. of Spectrosc.* **1999**, *3*, 39.

14. Wilson, E. B.; Decius, J. C.; Cross, P. C.; *Molecular Vibrations*, McGraw-Hill: New York, 1955.
15. Chantry, G. W.; In *The Raman Effect*, Vol. 1; Anderson, A.; Ed.; Marcel Dekker: New York, 1971, Chapter 2.
16. Karabatsos, G. J.; Hsi, N.; *J. Am. Chem. Soc.* **1965**, *87*, 2864.
17. Allinger, N. L.; Tribble, M. T.; Miller, M. A.; *Tetrahedron* **1972**, *28*, 1173.
18. Steinmetz, W. E. *J. Am. Chem. Soc.* **1976**, *96*, 685.
19. Cremer, D.; Binkley, J. S.; Pople, J. A. *J. Am. Chem. Soc.* **1976**, *98*, 6836.
20. Christian, S. D.; Grundes, J.; Klaeboe, P.; Torneng, E.; Woldbaek, T. *Acta Chem. Scand.* **1980**, *34A*, 391.
21. Strauss, H. L. *Annu. Rev. Phys. Chem.* **1983**, *34*, 301.
22. Caminati, W.; Scappini, F.; Damini, D. *J. Mol. Spectrosc.* **1984**, *108*, 287.
23. Durig, J. R.; Guirgis, G. A.; Krutules, K. A.; Phan, H.; Stidham, H. D. *J. Raman Spectrosc.* **1994**, *25*, 221.
24. Pouchert, C. J.; *The Aldrich Library of Infrared Spectra*, Edition III; 2nd Printing, Aldrich Chemical Company: Milwaukee, Wisc., 1981, Spectrum 10846-4 Cyclohexanecarboxaldehyde.